



Multifunctional wearable strain/pressure sensor based on conductive carbon nanotubes/silk nonwoven fabric with high durability and low detection limit

Yuxin He^{1,2} · Mengyang Zhou¹ · M. H. H. Mahmoud³ · Xushen Lu¹ · Guanyu He¹ · Li Zhang⁴ · Mina Huang⁵ · Ashraf Y. Elmagar⁶ · Qiang Lei¹ · Hu Liu² · Chuntai Liu² · Islam H. El Azab⁶

Received: 26 April 2022 / Revised: 19 June 2022 / Accepted: 20 June 2022 / Published online: 19 July 2022
© The Author(s), under exclusive licence to Springer Nature Switzerland AG 2022

Abstract

With the rapid development of flexible wearable strain sensor systems, electronic textiles with comfort and controllable strain/pressure-sensing capabilities have attracted great interest. However, it is still a great challenge to prepare multifunctional wearable strain/pressure sensor with an ultra-low detection limit through a facile and cost-effective method. Here, conductive carbon nanotubes modified silk nonwoven fabric (CNTs/SNWF) composite was successfully prepared by the surface micro-dissolution and adhesion technology (SD&AT). Micromorphology analysis showed that CNTs were adhered firmly on the surface of silk fiber to form an effective conductive network. The conductive CNTs/SNWF-based strain/pressure sensor can detect a strain as low as 0.05% and an ultralow pressure of 10 Pa, showing an ultrahigh discernibility. Besides, it also exhibited excellent sensing stability and reproductivity under different conditions, making it applicable in the field of real-time human movement monitoring. Moreover, electronic skin was also established based on the conductive CNTs/SNWF to recognize different tactile stimulus. Interestingly, the prepared conductive CNTs/SNWF also displayed great applicability for optical and thermal sensing, endowing it with more functionality for next-generation wearable electronics.

Keywords CNTs · Silk nonwoven fabric · Sensor · Human health monitoring · E-skin

✉ Yuxin He
heyx@haust.edu.cn

✉ Hu Liu
liuhu@zzu.edu.cn

¹ College of Chemical Engineering and Pharmaceutics, Henan University of Science and Technology, Luoyang, Henan 471023, People's Republic of China

² Key Laboratory of Materials Processing and Mold, Ministry of Education, National Engineering Research Center for Advanced Polymer Processing Technology, Zhengzhou University, Zhengzhou, Henan 450002, People's Republic of China

³ Department of Chemistry, College of Science, Taif University, Taif 21944, Saudi Arabia

⁴ College of Chemistry and Chemical Engineering, Luoyang Normal University, Luoyang 471934, Henan, China

⁵ College of Materials Science and Engineering, Taiyuan University of Science and Technology, Taiyuan 030024, China

⁶ Department of Food Science and Nutrition, College of Science, Taif University, Taif 21944, Saudi Arabia

1 Introduction

With the rapid development of artificial intelligence [1, 2], flexible strain/pressure sensors with the merits of light weight, fast response, wide response range, high stability, and high sensitivity have been widely applied in the fields such as wearable electronic products [3, 4], electronic skin (e-skin) [5, 6], intelligent robots [7, 8], and human-machine interfaces [9, 10]. Although traditional metal and inorganic semiconductor sensors show the merits of fast response, high sensitivity, and stability, its rigidity and limited sensing range can no longer meet the requirements of reagents when facing a variety of complex and special signals, which promote the development of flexible multifunctional strain/pressure sensor.

Compounding electroactive materials with flexible substrates is a shared method for preparing flexible strain/pressure sensors. Electroactive materials including polypyrrole [11], carbon nanotubes (CNTs) [12, 13], graphene (GR) [14, 15], silver nanowires (AgNW) [16, 17], and MXene [18, 19] are commonly adopted to prepare flexible strain

sensors. Among them, carbon-based materials are considered to be good candidates for manufacturing flexible strain sensors due to their lightweight, excellent mechanical properties, and high electrical conductivity. Therefore, scholars are committed to using carbon-based materials and flexible matrix composite to prepare flexible strain sensors. Recently, research on wearable flexible strain sensors prepared by hybridizing cotton [20], cellulose [21, 22], paper [23, 24], silk [25], and flexible polymer [26, 27] with CNT for human health monitoring and electronic skin has been widely reported. Zheng et al. [28] prepared a CNT/cotton strain sensor (CCSS) through multiple dipping processes, showing fast response time (~ 90 ms), excellent reproducibility, durability (10,000 cycles at 30% strain), and a low strain detection limit ($\sim 0.4\%$ strain). Therefore, natural flexible biomaterials can be used to prepare flexible strain/pressure sensors with excellent performance.

The unique advantages of silk fiber in structure and function make it have infinite possibilities in the field of flexible multifunctional strain/pressure sensor [29, 30]. Silk-based wearable strain/pressure sensors, especially for the resistive-type strain/pressure sensors with the characteristics of easy signal readout and simple structure design, have been developed for monitoring human motion and personal healthcare systems [31, 32]. Li et al. [33] fabricated a flexible and super-hydrophobic silk fibroin (SF) membrane by spraying polydimethylsiloxane (PDMS) solution with silver nanowires (AgNWs) on the surface of it, showing great application in flexible strain/pressure sensors and shielding in wet environments. Zhou et al. [34] prepared CNTs/silk fiber (CSF) with one-sided and high conductivity by the strategy of micro-dissolving the surface. The results show that CSF can be used as a flexible strain sensor for monitoring human motion. Besides, benefiting from the perfect conductive network and fibrous network structure, CSF displays high efficient Joule heating performances. Although all these reported silk-fabric-based flexible strain sensors demonstrate excellent flexibility and stability, however, its ability to detect small strain/pressure is poor, and the preparation processes are expensive and complicated, which hinder its large-scale production and wide applications [35]. Hence, it is still a challenge to prepare multifunctional wearable sensor with ultra-low detection limit of strain or pressure by a facile and cost-effective method.

In this study, the conductive carbon nanotubes modified silk nonwoven fabric (CNTs/SNWF) composite was successfully prepared by the surface micro-dissolution and adhesion technology (SD&AT), and its applications in wearable strain/pressure sensor, optical sensor, and thermosensitive sensor were systematically explored. Utilizing the micro-dissolution of sericin on the surface of silk fibers in the nonwoven fabric, the CNT nanofibers were strongly adhered to the surface of silk fiber, and an effective conductive network

was constructed by virtue of the natural three-dimensional structure of silk nonwoven fabric (SNWF). In order to estimate the application capacity of the conductive CNTs/SNWF as flexible strain/pressure sensor, uniaxial tensile/compressive sensing tests were carried out to study its sensitivity and sensing range, and cyclic tensile/compressive sensing tests were also carried out to characterize its response time, strain/pressure and rate dependence and long-term stability. Besides, the conductive CNTs/SNWF-based strain/pressure sensor was also applied to evaluate its applicability for monitoring human movement and physiological signals. What is more, the optical and thermal sensing performance of the conductive CNTs/SNWF were also systematically studied to broad its scope of application.

2 Experimental

2.1 Materials

Silk nonwoven fabrics (SNWF, 25.0 g/m^2) were obtained from Xiancan Silk Biotechnology Co., Ltd (Suzhou, China). Multi-walled carbon nanotubes (CNTs, TNM0, 98.0 wt.%) were purchased from Chengdu Organic Chemicals Co. Ltd., Chinese Academy of Sciences, China. Urea (99.5 wt.%), cyclohexane (99.9 wt.%), and ethanol (99.5 wt.%) were purchased from Aladdin Reagent Co., Ltd (Shanghai, China). Commercial interdigitated electrodes designed on polybutylene terephthalate (PBT) substrate were purchased from Shenzhen ChangMing Sensor Technology Co., Ltd, China (Figure S1). All the materials and reagents were used as received without any further treatment.

2.2 Preparation of conductive CNTs/SNWF

Figure 1a displays the diagram of preparation process for conductive CNTs/SNWF. Specifically, 5.0 g urea was dissolved into 100 g deionized water under magnetic stirring to obtain a transparent solution, followed by mixing 0.15 g CNTs under ultrasonic dispersion for 25 min to obtain a homogeneous black CNT dispersion. Then, pristine SNWF was cut into rectangle sample with a dimension of $3 \text{ cm} \times 5 \text{ cm}$ (Fig. 1b) and dipped into the prepared CNT dispersion under a temperature of $90 \text{ }^\circ\text{C}$. After certain time intervals (1 s, 5 s, 60 s, 300 s, and 900 s), all the samples were further washed with DI water and ethanol for five times and then placed on the polytetrafluoroethylene plate followed by drying in a vacuum oven at $40 \text{ }^\circ\text{C}$ for 5 h, obtaining the designed conductive CNTs modified SNWF (CNTs/SNWF) using the surface micro-dissolution and adhesion technology (SD&AT) (Fig. 1c).

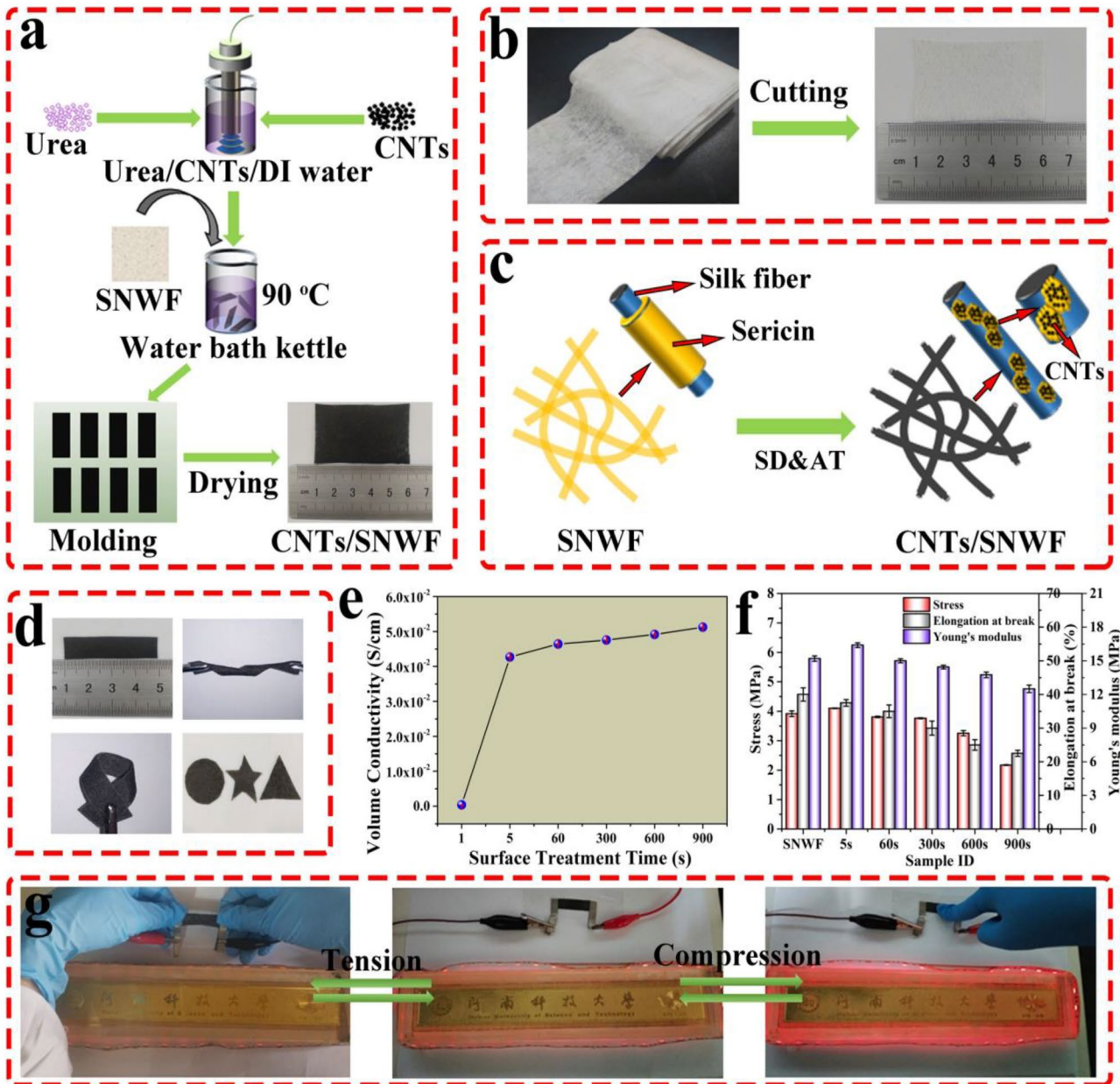


Fig. 1 Preparation of conductive CNTs/SNWF and its physical characteristics. **a** Schematic illustration for the preparation of conductive CNTs/SNWF. **b** Digital photos of pristine SNWF and the tailored sample. **c** Schematic illustration for SD&AP. **d** Digital photos of CNTs/SNWF with good twistability and bendability. **e** Conductivity

of CNTs/SNWF as a function of surface treatment time. **f** The tensile mechanical properties of CNTs/SNWF with different surface treatment time under 1% tensile strain at a tensile rate of 5 mm/min. **g** The light intensity variation of LED upon the tension and compression of the connected CNTs/SNWF

2.3 Characterization

The conductive CNTs/SNWF was cut into a rectangle sample with a dimension of 1 cm x 4 cm, and both ends of the sample were coated with conductive silver paste and adhered with the conductive tape to fabricate the flexible CNTs/SNWF strain/pressure sensor. Strain/pressure-sensing properties of the conductive CNTs/SNWF were evaluated by the self-built

equipment as shown in Figure S2. Carl Zeiss Sigma 500 field emission scanning electron microscopy was adopted to characterize the micromorphology of samples. X-ray diffraction (XRD) patterns within the 2θ scope of 10~80° were recorded on a D8 ADVANCE diffractometer (Bruker Instruments Co., Germany). Raman spectrum was measured by a Raman spectrometer (Renishaw inVia, Renishaw Company, UK). Thermogravimetric analysis (TGA) was performed on a TGA 2

(Mettler Toledo Instruments Co., Switzerland) system from room temperature to 800 °C with heating rate of 10 °C/min under nitrogen atmosphere. Digital Multimeter (DMM4040, Tektronix Technology Co., Ltd., China) was used to measure the conductivity of samples. Tensile/compressive mechanical performance of the samples was assessed by a single-column micro-control electronic universal testing machine (WWD-1D, Jilin Guanteng Automation Technology Co., Ltd., China). I–V curves of the sample under different strain/pressure were tested by Princeton ParStat4000 + electrochemical workstation (AMETEK shanghai trading Co., Ltd., China).

3 Results and discussion

Due to the excellent flexibility of the original SNWF, the prepared CNTs/SNWF shows good twistability, bendability, and tailorability (Fig. 1d), making it applicable for wearable electronic device. Sericin is water-soluble and easily soluble in hot water, acid, and alkali solutions [29, 34]. By controlling the degree of dissolution of sericin, a conductive filler can be adhered to the surface of silk fiber to construct a conductive network. Figure 1e displays the relationship between conductivity and surface treatment time, where the conductivity increases significantly from 3.76×10^{-4} s/cm for 1 s to 4.32×10^{-2} s/cm for 5 s and then tends to be stable with further increasing surface treatment time. Such a surface treatment time-dependent conductivity can be clarified based on the SEM images shown in Figure S3, where the amount of CNTs adhered to the fiber surface increases significantly as the surface treatment time increases from 1 to 5 s (Figure S3a, b), and no obvious change is observed with further increasing the surface treatment time (Figure S3c–g), demonstrating the construction of stable and perfect conductive network. Figures 1f and S4 show the effect of surface treatment time on the tensile mechanical performance of conductive CNTs/SNWF. Obviously, both the tensile stress and Young's modulus display a slight increase under a surface treatment time of 5 s, but they exhibit an obvious decrease trend with increasing surface treatment time. When the surface treatment time is 5 s, the sericin on the surface of silk fibroin fiber is slightly dissolved and a layer of CNTs is adhered to its surface. Under the synergistic effect of CNTs and sericin, the tensile strength and Young's modulus of silk fibroin fibers were improved. When the surface treatment time is further extended, the physical interaction between silk fibroin fibers is weakened due to degumming, such as hydrogen bond or van der Waals force [36, 37], which speeds up the fracture of silk fibroin fibers. Besides, the elongation at break also shows a downward trend when the surface treatment time is extended from 5 to 900 s. Considering the stable conductivity and comprehensive mechanical property, CNTs/SNWF with a surface treatment time of 5 s was applied

for the subsequent study. Furthermore, as shown in Fig. 1g, the prepared conductive CNTs/SNWF was inserted in red light-emitting diode (LED) circuits, and the brightness of LEDs decreases when the external tension is applied to the CNTs/SNWF and then becomes normal after the tension is removed. When the external pressure is applied to the CNTs/SNWF, the brightness of the LED can also become brighter and then recover to normal after the pressure is removed. All these indicate the great potential of our prepared conductive CNTs/SNWF to be served as strain/pressure sensor.

Then, the microstructure of original SNWF and conductive CNTs/SNWF were systematically investigated. As displayed in Fig. 2a–a₃, the original SNWF shows the entangled fiber network, of which the smooth silk fiber surface is wrapped with a layer of sericin [38, 39]. After the decoration with CNTs, it can be seen clearly from Fig. 2b–b₃ that partial sericin on the silk fiber surface is dissolved by the urea solution and forms micro-cracks, and CNTs are homogeneously adhered with the remaining undissolved sericin. Hence, a proper surface treatment time is important to enable a slightly soluble sericin on the surface, which acts as a binder to firmly fix the CNT onto the surface of SNWF, constructing effective conductive layer. The micro-cracks formed by sericin micro-dissolution on the surface of silk fiber can have a positive effect on improving the sensitivity of conductive CNTs/SNWF [24, 31]. According to the cross-sectional SEM images shown in Fig. 2c–c₃, it can be obtained that the thickness of CNTs/SNWF is about 515 μm, where the silk fibers are “point to point” contact with each other, constructing effective conductive network for the prepared CNTs/SNWF.

Figure 2d displays the XRD patterns of SNWF and CNTs/SNWF, and two characteristic diffraction peaks at 29.0° and 20.5°, which are corresponded to the molecular structure of Silk I and Silk II for silk fibroin, are clearly observed for SNWF [40]. After the surface modification treatment, the peak of Silk I molecular structure almost disappears for CNTs/SNWF, indicating the decrease in the proportion of Silk I due to the degumming treatment. Besides, the peak intensity of Silk II molecular structure also weakens, and the (002) diffraction peak of the hexagonal graphite of CNTs at 26.5° is not observed, which can be ascribed to the strong interfacial interaction between Silk fiber and CNTs that led to the shift of the diffraction peak of CNTs to merge with the diffraction peak of Silk II [41]. As for the Raman spectroscopy shown in Fig. 2e, the SNWF shows no obvious peaks due to the mixed composition and disordered internal structure [42], but two additional distinct bands at 1601.5 cm⁻¹ and 1319.7 cm⁻¹ corresponding to the G-band and D-band of CNTs are clearly observed for CNTs/SNWF, confirming the successful decoration of CNTs, which is consistent with the results reported in other literatures [43]. Figures 2f and S5 show the thermogravimetric performance of SNWF

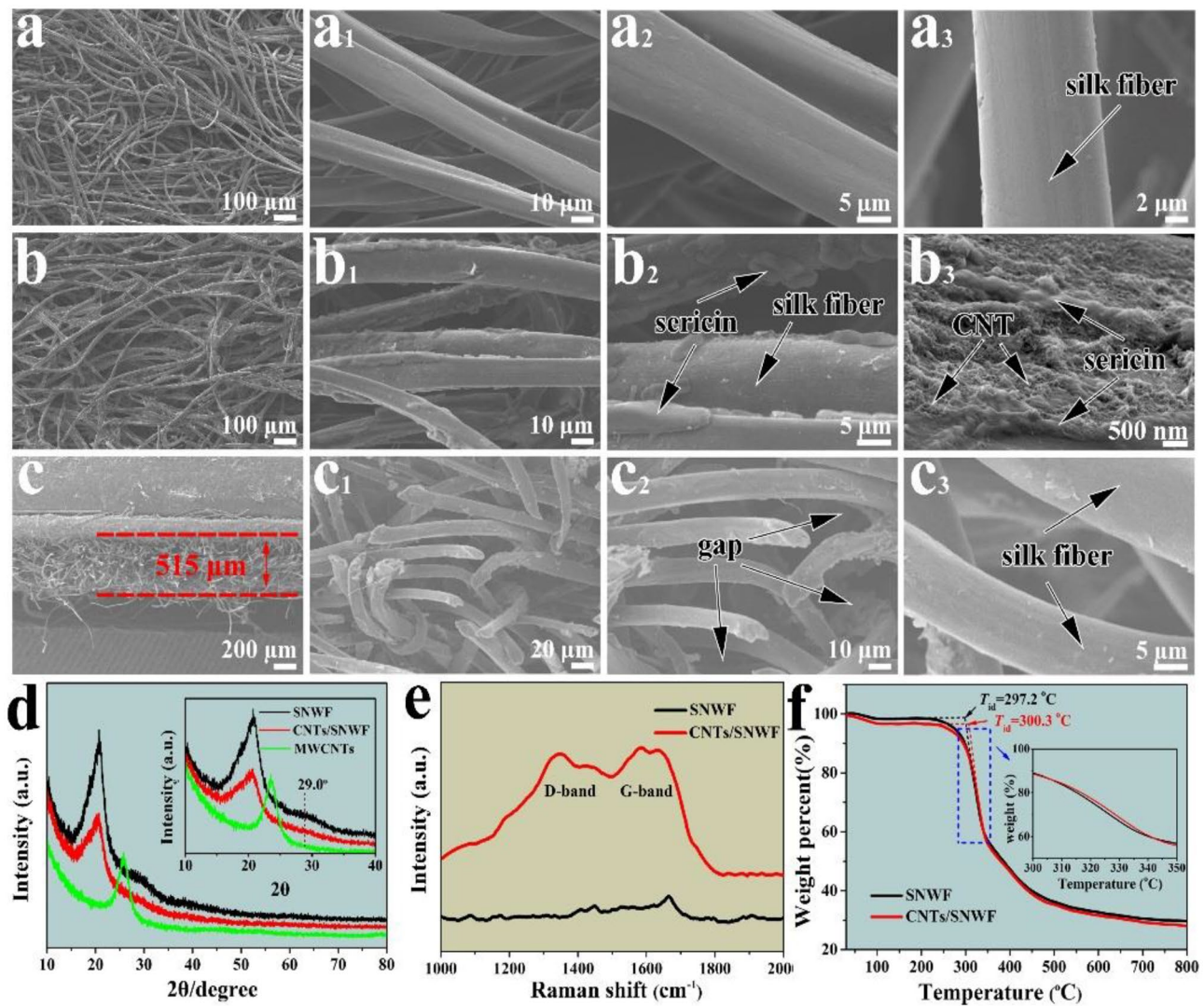


Fig. 2 Morphology and structure characterizations of original SNWF and conductive CNTs/SNWF. SEM images of **a**~**a**₃ original SNWF and **b**~**b**₃ conductive CNTs/SNWF at different magnifications. **c**~**c**₃

Cross-sectional SEM images of conductive CNTs/SNWF at different magnifications. **d** XRD patterns, **e** Raman spectra, and **f** TG curves of original SNWF and conductive CNTs/SNWF

and CNTs/SNWF, and the onset decomposition temperature (T_{onset}), maximum decomposition temperature (T_p), and residual carbon content of them are listed in Table S1. Clearly, SNWF and CNTs/SNWF exhibit the similar thermal decomposition properties, and the T_{id} and T_p of them are 297.2 °C and 327.5 °C and 300.3 °C and 329.0 °C, respectively, indicating that the thermal stability of SNWF can be well kept without being destroyed after being treated with surface micro-soluble degumming and adhesion modification technique. In addition, it can be seen that the final mass of original SNWF is slightly higher than that of the CNTs/SNWF. Due to the excellent thermal conductivity of CNTs, the thermal absorption capacity of CNTs/SNWF composites is improved after a small amount of adhesion on the surface of silk fibroin, resulting in a slight decrease in the final mass.

The tensile strain-sensing performances of prepared conductive CNTs/SNWF were first investigated. As depicted in Figure S6, the strain sensor with 5-s surface treatment time exhibits optimal sensitivity and working range. Subsequently, gauge factor ($GF = (\Delta R/R_0)/\varepsilon$, $\Delta R = (R - R_0)$, R_0 and R represent the initial resistance and instantaneous resistance, ε stands for the tensile strain) [44] was adopted to evaluate the strain sensitivity of the sensor with a surface treatment time of 5 s. As shown in Fig. 3a, the whole sensing range can be divided into three typical stages, of which the GF is calculated to be about 8, 74, and 7000 in the strain range of $\varepsilon < 5\%$, $5\% \leq \varepsilon < 35\%$, and $\varepsilon \geq 35\%$, respectively. It is well known that the sensitivity of strain sensor is closely related to the variation of conductive network structure during the tensile process, which can be well understood

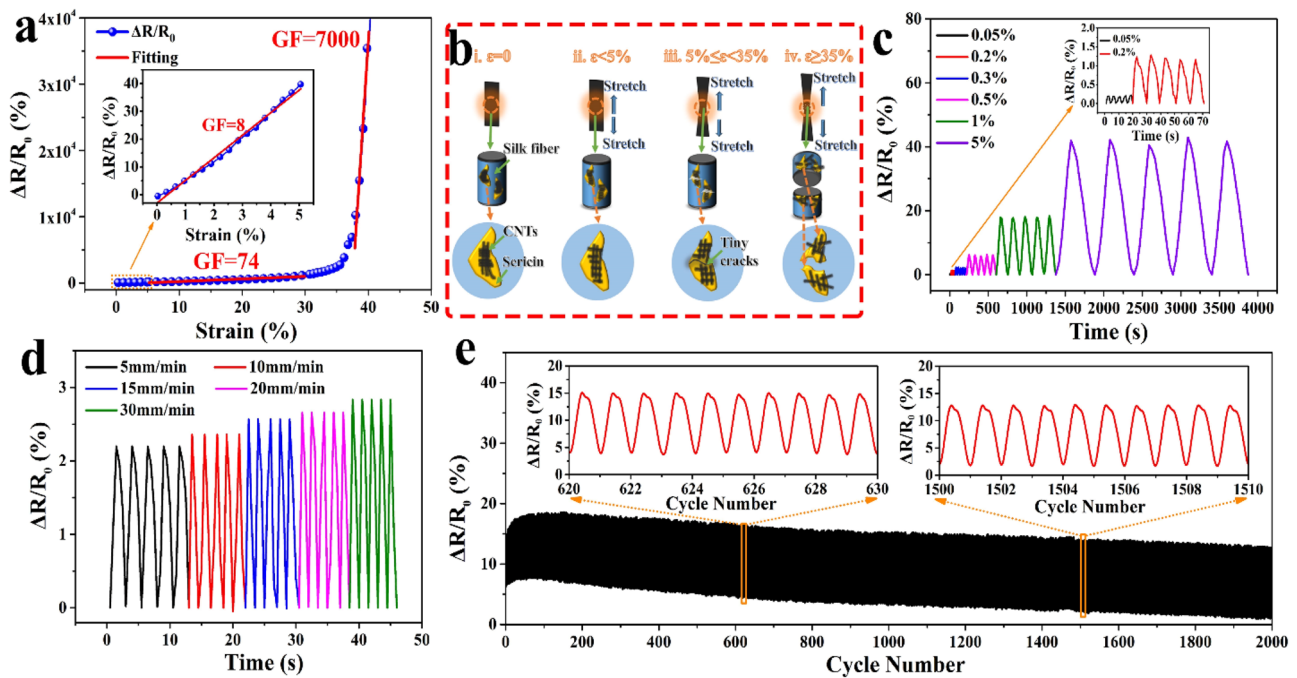


Fig. 3 Tensile strain sensing performance of CNTs/SNWF-based strain sensor. **a** $\Delta R/R_0$ vs. strain for the strain sensor with 5-s surface treatment time at a tensile rate of 5 mm/min. **b** Schematic diagram of the strain-sensing mechanism of the strain sensor. **c** Cyclic strain-sensing behavior of the strain sensor under different strain amplitudes

at a tension rate of 5 mm/min. **d** Cyclic strain-sensing behavior of the strain sensor under 1% strain at different tension rates. **e** Long-term stability and reliability of the strain sensor at a tensile rate of 5 mm/min in 2000 cycles

through the corresponding schematic diagram (Fig. 3b) and SEM images (Figure S7). In the initial 5% strain, the tangled conductive silk fibers are rearranged along the stretching direction (Figs. 3b-ii and S7a~a₂), the separation between adjacent fibers generates subtle variation in the conductive network, so a lower sensitivity is obtained. With further increasing to the strain range of 5–35%, the adhered CNTs conductive layer on the silk fiber surface is broken into some microcracks (Figs. 3b-iii and S7b~b₂), resulting in the significant destruction of the conductive network and a higher sensitivity. When the strain is larger than 35%, the propagation of microcracks leads to the formation of isolated fragments, and some silk fibers are also pulled apart due to the poor mechanical property (Figs. 3b-iv and S7c~c₂). All these can cause the complete destruction of conductive network gradually, exhibiting a sharp increase of resistance and the highest sensitive strain range.

The cyclic strain-sensing performance of the conductive CNTs/SNWF with a surface treatment time of 5 s were systematically characterized. It can be clearly seen in Figure S8 that the I–V curves of the strain sensor with different strain amplitudes exhibit good linear ohmic behavior, indicating the excellent stable electrical property which is conducive to stable signal output and sensing properties. As shown in Figs. 3c and S9, the strain sensor displays stable and repeatable sensing behavior in the strain range of 0.05–25%, and

the sensing peak value shows an upward trend with increasing strain amplitude, which is coincided with the result in Fig. 3a. It is worth mentioning that the sensor can detect a strain as low as 0.05% due to the constructed fractured structure. Besides, the special “shoulder peak” appears for the sensing pattern under higher strain (Figure S9), which can be ascribed to the competition between the destruction and reconstruction of the conductive fabric network structure during cyclic stretching. Specifically, the longitudinal stretching of conductive fiber under small strain (<5%) cause the subtle and stable variation of conductive network (Figure S9b-ii), but the separation of the fractured fiber and the overlap between adjacent fibers occur simultaneously under large strain (>5%) (Figure S9b-iii), the competition between them leads to the unstable variation of conductive network, resulting in the “shoulder peak.”

Figure 3d shows the cyclic strain sensing behavior of the strain sensor at 1% strains under different tension rates. Obviously, stable sensing pattern is obtained for a fixed strain rate, but it displays an increasing trend with increasing strain rate. Such a strain rate–dependent response performance can be clarified by the stress vs. strain curves illustrated in Figure S10, where the strain sensor endures larger stress under higher rate, causing more serious damage to the conductive network and higher response. As shown in Figure S11, when an instantaneous tensile strain of 1% is

exerted on the sensor at a rate of 5 mm/min, the response and recovery time is 86 ms and 117 ms, respectively [45]. Finally, the long-term fatigue resistance of the strain sensor in 2000 stretching cycles was also investigated. As depicted in Figs. 3e and S12, the strain sensor displays excellent stability and recoverability during 2000 stretching-releasing cycles or after water washing, which is mainly ascribed to the good long term cyclic mechanical fatigue resistance of the strain sensor (Figure S13).

Subsequently, pressure sensing performance of the conductive CNTs/SNWF-based pressure sensor was further investigated. Figure 4a shows the $-\Delta R/R_0$ vs. stress curve of the pressure sensor, where the $-\Delta R/R_0$ value increases significantly with increasing pressure in range of 0~4.5 kPa and then gradually tends to be stable. The insert shows the pressure sensitivity (S , $S = (-\Delta R/R_0)/P$, where P represents the applied pressure) of the pressure sensor [46], displaying the similar trend with Fig. 4a. As displayed in Figs. 4b and S14, the pressure-sensing behavior of the strain sensor is attributed to the change of the three-dimensional fibrous structure. Within the initial pressure range of 0~1.0 kPa, the uncontacted conductive silk fibers turn to be “point to point” contact under the action of external pressure, and the $-\Delta R/R_0$ value of the sensor increases sharply, resulting in a sharp increase of S value (Figs. 4b-ii and S14a-a₂). As the pressure

further increases to 4.0 kPa, the contact mode between adjacent fibers becomes to be “face to face” contact (Figs. 4b-iii and S14b-b₂), and the construction of new conductive network slows down, showing a decreasing trend in pressure sensitivity. Finally, the conductive network enters the dense zone, where silk fibers are tightly stacked, and the resistance of the sensor shows a slow exponential decline trend and then tends to be stable (Figs. 4b-iv and S14c-c₂). After that, the cyclic pressure-sensing behaviors of the strain sensor were also systematically characterized. In Figure S15, the pressure sensor exhibits good linear I–V curves under different pressures, indicating its stable electrical performance, which is conducive to stable signal output and sensing performance. As illustrated in Fig. 4c, the pressure sensor exhibits stable and repeatable sensing pattern under different pressures in the stress range of 0.01~13 kPa, and a slight pressure change of 10 Pa can also be effectively detected, showing an ultrahigh discernibility. Meanwhile, stable and repeatable sensing pattern was also observed for the pressure sensor under different compression rates (Fig. 4d), and the sensing peak also exhibits increasing trend with increasing compression rate, which can be explained by the larger pressure under a higher rate (Figure S16). Furthermore, the response time and recovery time of the pressure sensor is 55 ms and 40 ms, respectively (Figure S17). Finally, the

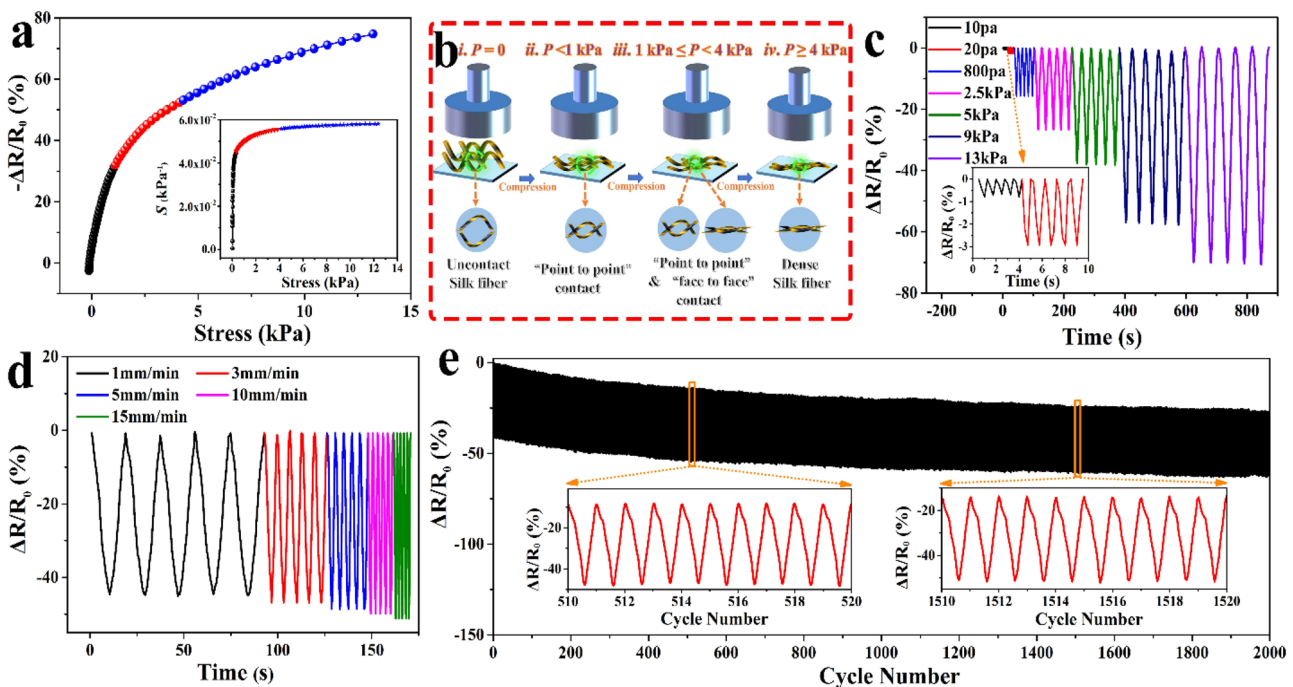


Fig. 4 Pressure sensing performances of the conductive CNTs/SNWF-based pressure sensor. **a** $-\Delta R/R_0$ and (insert) pressure sensitivity S vs. stress for the pressure sensor with 5-s surface treatment time at a compressive rate of 3 mm/min. **b** Schematic diagram of the compressive sensing mechanism of the pressure sensor. **c** Cyclic pressure

sensing behavior of the pressure sensor under different pressures. **d** Cyclic pressure sensing behavior of the pressure sensor under a pressure of 5.0 kPa at different compression rates. **e** Long-term stability and reliability of the pressure sensor at a compression rate of 3 mm/min in 2000 cycles

pressure sensor also shows good stability and recoverability after 2000 compression cycles (Fig. 4e), which is also supported by its excellent compression mechanical properties shown in Figure S18. In summary, as shown in Table S2, the conductive CNTs/SNWF-based strain/pressure sensor shows superior sensing performance than other reported works.

Aiming to verify the application prospects of conductive CNTs/SNWF-based strain/pressure sensor, it was adhered to the elbow and finger by medical tape to detect the signals of joint movement. As depicted in Fig. 5a and b, the sensor outputs stable cyclic sensing signal under a fixed bending angle and the responsiveness increases with increasing the bending angle, indicating the ability to detect different bending motions. In addition, the sensor was also applied to detect weak signals produced by tiny deformation of human body. When the sensor was adhered to the brachioradialis of forearm (Fig. 5c), the sensing signal increases with the muscle tension and recovers to the initial value as releasing the muscle, which proves its potential application value in guiding human body training and injured muscle recovery. As we all know, real-time monitoring of the pulse is an important indicator of cardiovascular disease detection. Here, as shown in Fig. 5d, the sensor also can monitor the pulse signal of human body, and regular sensing signal is acquired. In detail, the volunteer's pulse is calculated as 75 beats per minute, which is within the range of normal

human pulse level. In addition, the insert figure exhibits an enlarged view of one pulse signal, where three distinguishable peaks of the percussion wave (P1), the tidal wave (P2) and the dicrotic wave (P3) were observed [47], indicating the superior sensitivity and fast response of the sensor. As shown in Fig. 5e, when the volunteer stepped on the sensor fixed on the ground with his heel, the resistance decreased. When the heel left the sensor, the resistance increased. The output signal was stable throughout the test. This provides a method for detecting the flow of people in public places. When the sensor is pressed quickly within a certain time interval, the sensor shows excellent signal responsiveness and stability (Fig. 5f), providing technical support for detecting rapid human movement and predicting early Parkinson's disease [48, 49]. Based on the testes conducted above, it can be claimed that our prepared conductive CNTs/SNWF-based strain/pressure sensor has huge potential application in human health monitoring and movement monitoring.

The prepared conductive CNTs/SNWF was placed between the two PDMS films and an interdigitated electrode designed on PBT supporting pad to assemble electronic skin (e-skin) with a sandwich structure (Fig. 6a), and the assembled e-skin with 4×4 pixels show excellent flexibility and conformability (Fig. 6b). Due to the excellent flexibility of the prepared e-skin, it can be arbitrarily curled and tightly attached to the body to detect external

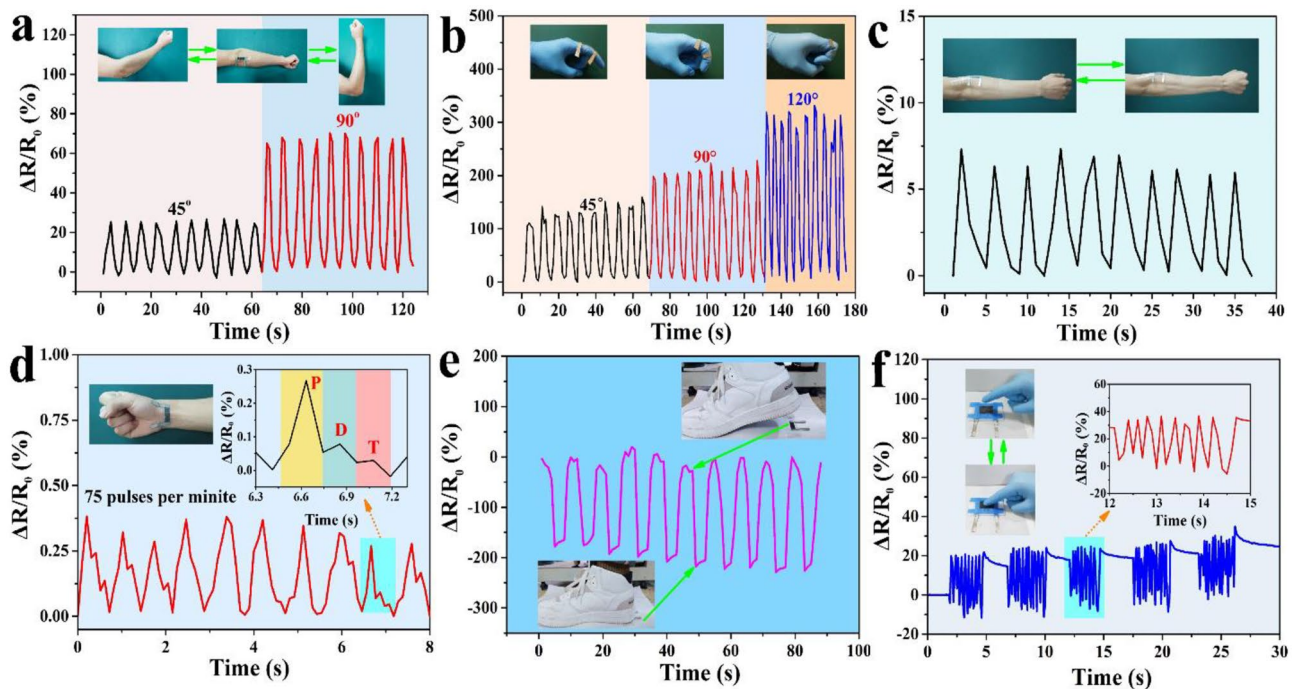


Fig. 5 Applications of the conductive CNTs/SNWF-based strain/pressure sensor. Sensing performances of the sensor for the real-time detection of **a** knee bending, **b** finger bending, **c** elbow bending, **d** brachioradialis of the forearm for tensing and relaxing, **e** and **f**

wrist pulse. **g** Real-time sensing signal recording of the sensor upon heel stepping for the volunteer. **h** and **i** Real-time sensing signal of the sensor for pressing quickly within a certain time interval

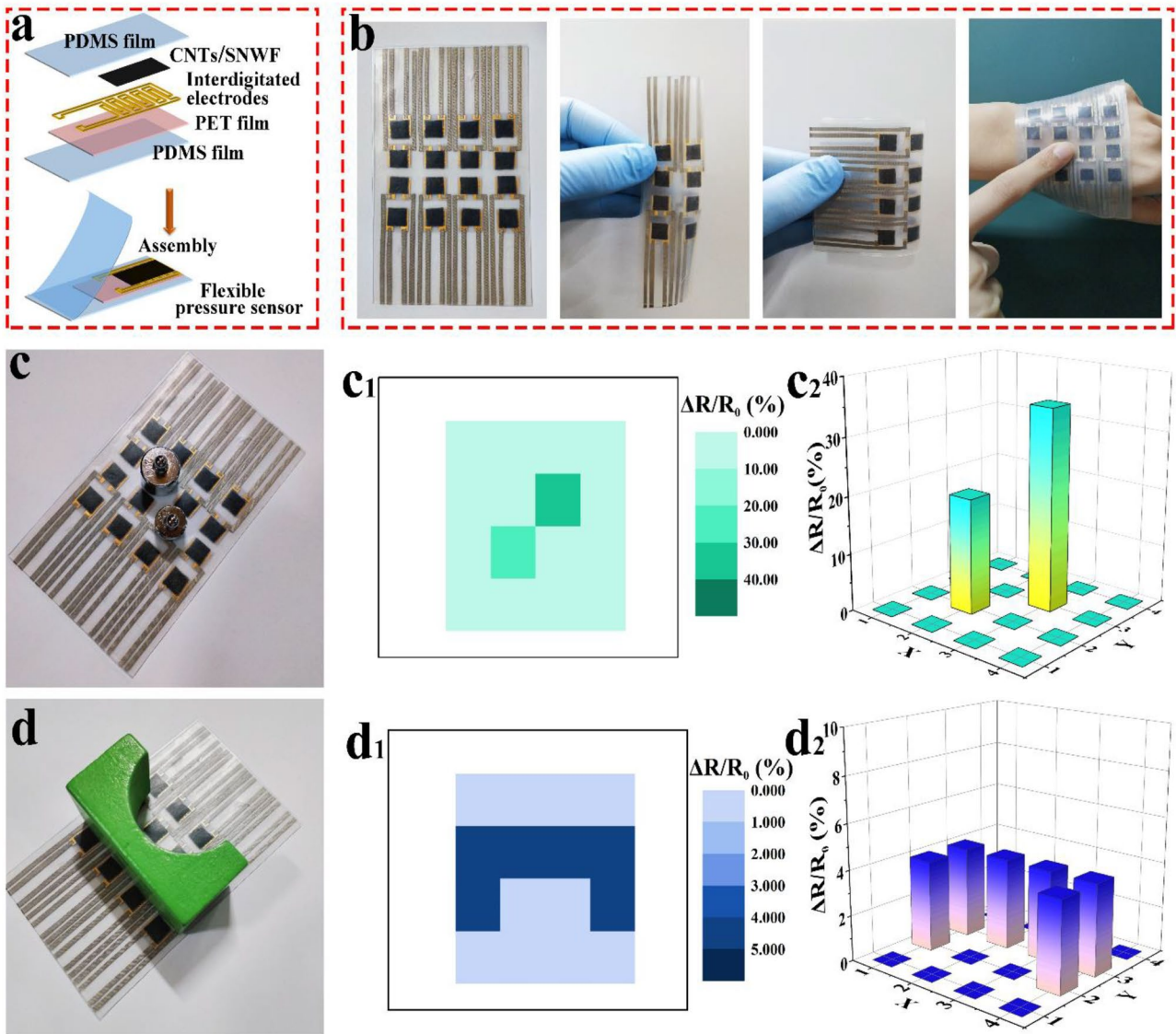


Fig. 6 Application of the conductive CNTs/SNWF-based pressure sensor in intelligent e-skin. **a** Schematic diagram of the e-skin structure. **b** Photographs of the assembled e-skin. **c** Photograph of a 50-g weight and a 20-g weight lying onto the e-skin and (c₁, c₂) the cor-

responding pressure sensing mapping based on the resistance variation. **d** Photograph of an “arch bridge” brick lying onto the e-skin and (d₁, d₂) the corresponding pressure distribution mapping based on the resistance variation

loads. Applications of the e-skin for detecting different pressure signals and mapping the spatial pressure distribution were also investigated. As expected, when weights of different masses are placed on the e-skin (Fig. 6c), the e-skin can also accurately recognize its position and weight according to the pressure sensing signal, which can be acquired from the resistance variation of each pixel (Fig. 6c1–c2). Meanwhile, based on the spatial pressure distribution, the shape and position of the “arch bridge” brick placed flat on e-skin can also be accurately recognized (Fig. 6d–d2). As a result, our prepared conductive CNTs/SNWF-based pressure sensor has great potential for flexible e-skin.

Optical and thermal response of the conductive CNTs/SNWF were further conducted to explore its other potential applications. Figures 7a and S19a exhibit the schematic diagram and digital images of the method and mechanism for the optical sensing performance of the conductive CNTs/SNWF, and the height of the xenon lamp was adjusted to simulate different light intensities (14.5 cm is equal to 1 light intensity, 9.5 cm is equal to 3 light intensities, 7.2 cm is equal to 5 light intensities) [50, 51]. Figure 7a1 shows the sensing behavior of the conductive CNTs/SNWF irradiated by different light intensities, of which the irradiation time is fixed at 5 s. It can be observed that the responsiveness of conductive CNTs/SNWF increases with the increase of light

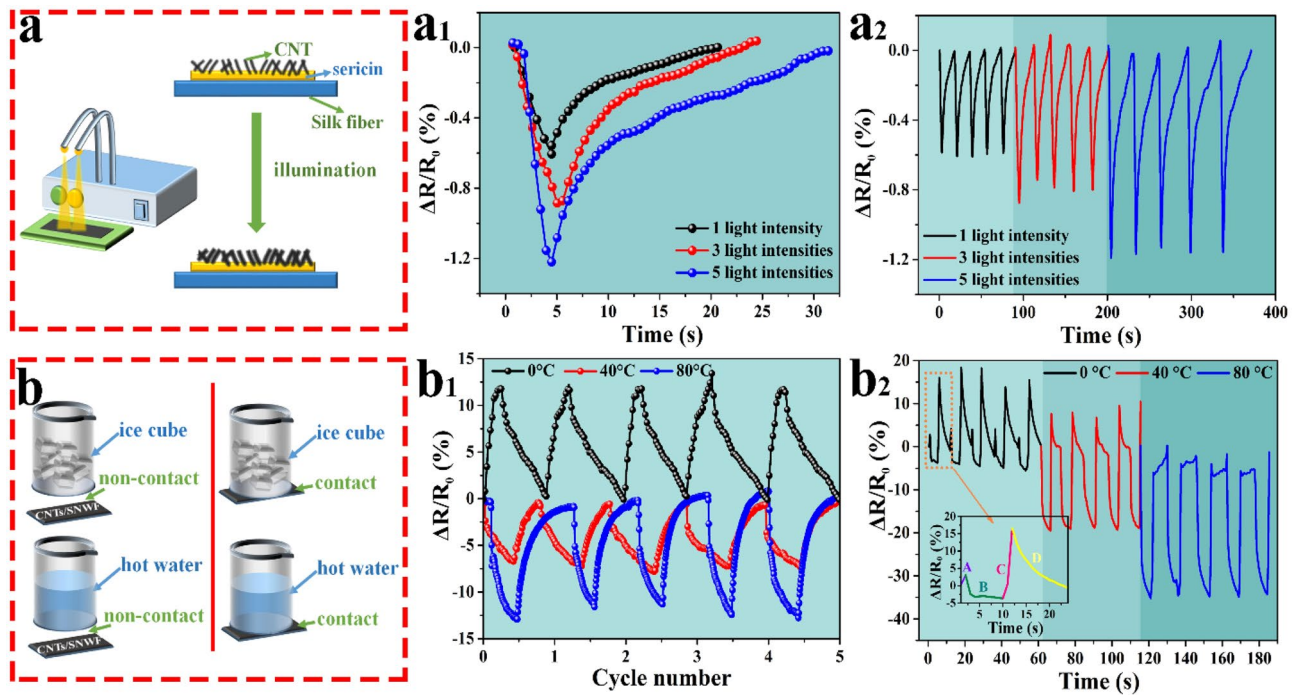


Fig. 7 The application of the conductive CNTs/SNWF for **a** optical and **b** thermal response. **a₁** Resistance variation vs. time of the conductive CNTs/SNWF irradiated by different light intensities. **a₂**

Cyclic optical sensing behavior the conductive CNTs/SNWF under different light intensities. **b₁** The non-contact mode and **b₂** the contact mode temperature responsiveness of conductive CNTs/SNWF

intensities, and a longer recovery time to its initial value. In addition, as shown in Fig. 7a2, the conductive CNTs/SNWF exhibits stable and repeatable sensing pattern under different light intensities. Essentially, the response behavior of the conductive CNTs/SNWF after being exposed to light can be attributed to the increase of the carrier concentration, which is consistent with the literatures [52].

For the thermal sensing performance of the conductive CNTs/SNWF, the non-contact and contact modes were systematically investigated at the room temperature of 20 °C, and their testing devices are shown in Figs. 7b and S19b~c₂. For the 0 °C beaker, the conductive CNTs/SNWF under both non-contact and contact modes exhibit an increase of the $\Delta R/R_0$ (Fig. 7b1 and b2). After moving away from the conductive CNTs/SNWF, the $\Delta R/R_0$ returns to its original value. As for the higher temperature beaker (40 °C and 80 °C) that lead to the increased electron migration rate, lower resistance was obtained. The $\Delta R/R_0$ can also return to its original value after moving away the heat source. The thermal response behavior of the conductive CNTs/SNWF at different temperatures can be attributed to the intrinsic negative TCR effect of it, which is consistent with the literature [53]. Moreover, the conductive CNTs/SNWF exhibits good stable and repeatable sensing mode under different temperatures, demonstrating the excellent non-contact and contact thermal sensing characteristics. Due to the thermal sensing characteristic of the conductive CNTs/SNWF, the strain/

pressure sensing properties of the conductive CNTs/SNWF at different temperatures were also investigated. As shown in Figure S20, the strain/pressure sensor at both low temperatures (−65 °C) and high temperatures (50 °C, 100 °C, and 200 °C) also displays excellent stability and repeatability. But it displays different responsiveness due to the thermal sensing characteristic, supplying a calibration basis for the strain/pressure sensor under different application scenario. In summary, the conductive CNTs/SNWF has huge potential applications in advanced flexible smart electronic skins and human–machine interfaces for next-generation wearable electronic devices.

4 Conclusion

Carbon nanotube modified silk nonwoven fabric (CNTs/SNWF) composite was prepared by a simple surface micro-dissolution and adhesion technology (SD&AT), and the designed conductive CNTs/SNWF-based flexible strain/pressure sensor showed good sensing performance in detecting small limits. The sensor can detect a strain as low as 0.05% and an ultralow pressure of 10 Pa, showing an ultrahigh discernibility. In uniaxial tension and compression tests, the sensor exhibited linear I–V property and fast responsive times (86 ms in strain sensing and 55 ms in pressure sensing). In the cyclic tension and compression

sensing tests, the sensor also showed good reproducibility, reliability, and durability. Moreover, the conductive CNTs/SNWF-based strain/pressure sensor can identify various human movement and health signals, such as leg, arm, and finger bending, early-stage Parkinson's static tremor, and wrist pulse. Furthermore, the conductive CNTs/SNWF can be integrated into an e-skin to monitor various pressure signals and map the spatial pressure distribution and also be used as the optical and thermosensitive sensor. In summary, the conductive CNTs/SNWF has huge potential applications in advanced flexible smart electronic skins and human–machine interfaces for next-generation wearable electronic devices.

Supplementary Information The online version contains supplementary material available at <https://doi.org/10.1007/s42114-022-00525-z>.

Funding The research was financially supported by the National Natural Science Foundation of China (NO: U1604253, NO: 51803191), Key Scientific and Technological Project of Henan Province—China (202102210038, 202102210043), the Student Research Training Plan of Henan University of Science and Technology—China (2021144), and Taif University Researchers Supporting Project (TURSP-2020/158), Taif University, Taif, Saudi Arabia.

Declarations

Competing interests The authors declare no competing interests.

References

- Huang H, Han L, Wang Y, Yang Z, Xu M (2020) Tunable thermal-response shape memory bio-polymer hydrogels as body motion sensors. *Eng Sci* 9:60–67
- Gao SL, Zhao XH, Fu Q, Zhang TC, Zhu J, Hou FH, Ni J, Zhu CJ, Li TT, Wang YL, Murugadoss V, Mersal GAM, Ibrahim MM, El-Bahy ZM, Huang MN, Guo ZH (2022) Highly transmitted silver nanowires-SWCNTs conductive flexible film by nested density structure and aluminum-doped zinc oxide capping layer for flexible amorphous silicon solar cells. *J Mater Sci Technol* 126:152–160
- Pan D, Yang G, Abo-Dief H, Dong J, Su F, Liu C, Li Y, Xu B, Murugadoss V, Naik N, El-Bahy S, El-Bahy Z, Huang M, Guo Z (2022) Vertically aligned silicon carbide nanowires/boron nitride cellulose aerogel networks enhanced thermal conductivity and electromagnetic absorbing of epoxy composites. *Nano-Micro Lett* 14:118
- He Y, Wu D, Zhou M, Zheng Y, Wang T, Lu C, Zhang L, Liu H, Liu CT (2021) Wearable strain sensors based on a porous polydimethylsiloxane hybrid with carbon nanotubes and graphene. *ACS Appl Mater Interfaces* 13(13):15572–15583
- Yan X, Liu J, Khan MA, Sheriff S, Guo Z (2020) Efficient solvent-free microwave irradiation synthesis of highly conductive polypropylene nanocomposites with lowly loaded carbon nanotubes. *ES Mater Manuf* 9:21–33
- Zhao ZY, Zhao RX, Bai PK, Du WB, Guan RG, Tie D, Naik NH, Huang MN, Guo ZH (2022) AZ91 alloy nanocomposites reinforced with Mg-coated graphene: phases distribution, interfacial microstructure, and property analysis. *J Alloys Compd* 902:163484
- Jing C, Zhang YF, Zheng JJ, Ge SS, Lin J, Pan D, Naik N, Guo ZH (2022) In-situ constructing visible light CdS/Cd-MOF photocatalyst with enhanced photodegradation of methylene blue. *Particuology* 69:111–122
- Zhao YH, Liu KX, Hou H, Chen LQ (2022) Role of interfacial energy anisotropy in dendrite orientation in Al-Zn alloys: a phase field study. *Mater Des* 216:110555
- Yu Z, Yan Z, Zhang F, Wang J, Shao Q, Murugadoss V, Alhadrami A, Mersal G, El-Bahy Z, Li Y, Huang M, Guo Z (2022) Waterborne acrylic resin co-modified by itaconic acid and γ -methacryloxypropyl triisopropoxidesilane for improved mechanical properties, thermal stability, and corrosion resistance. *Prog Org Coat* 168:106875
- Liu H, Chen X, Zheng Y, Zhang D, Zhao Y, Wang C, Pan C, Liu C, Shen C (2021) Lightweight, superelastic, and hydrophobic polyimide nanofiber/MXene composite aerogel for wearable piezoresistive sensor and oil/water separation applications. *Adv Funct Mater* 31(13):2008006
- Chen Y, Lin J, Mersal GAM, Zuo JL, Li JL, Wang QY, FYH, Liu JW, Liu ZL, Wang B, Xu BB, Guo ZH (2022) Several birds with one stone? strategy of pH/thermo-responsive flame-retardant/photothermal bactericidal oil-absorbing material for recovering complex spilled oil. *J Mater Sci Technol* 128:82–97
- He Y, Chen Q, Wu D, Zhou M, Wang T, Lu C, Zhang L, Liu H, Liu C (2021) Effect of multiscale reinforcement by fiber surface treatment with polyvinyl alcohol/graphene oxide/oxidized carbon nanotubes on the mechanical properties of reinforced hybrid fiber composites. *Compos Sci Technol* 204:108634
- Zhang C, Li H, Huang A, Zhang Q, Rui K, Lin H, Sun G, Zhu J, Peng H, Huang W (2019) Rational design of a flexible CNTs@PDMS film patterned by bio-inspired templates as a strain sensor and supercapacitor. *Small* 15:1805493
- Nie B, Huang R, Yao T, Zhang Y, Miao Y, Liu C, Liu J, Chen X (2019) Textile-based wireless pressure sensor array for human-interactive sensing. *Adv Funct Mater* 29(22):1808786
- He Y, Chen Q, Liu H, Zhang L, Wu D, Lu C, OuYang W, Jiang D, Wu M, Zhang J (2019) Friction and wear of MoO₃/graphene oxide modified glass fiber reinforced epoxy nanocomposites. *Macromol Mater Eng* 304:1900166
- Zahid M, Zych A, Dussoni S, Spallanzani G, Donno R, MaggFiali M, Athanassiou A (2021) Wearable and self-healable textile-based strain sensors to monitor human muscular activities. *Compos B Eng* 220:108969
- Cheng T, Li X, Li S, Yan X, Zhang X, Wang F (2020) Surface plasmon resonance temperature sensor based on a photonic crystal fiber filled with silver nanowires. *Appl Opt* 59(17):5108–5113
- Liu H, Li Q, Zhang S, Yin R, Liu X, He Y, Dai K, Shan C, Guo J, Liu C, Shen C, Wang X, Wang N, Wang Z, Wei R, Guo Z (2018) Electrically conductive polymer composites for smart flexible strain sensors: a critical review. *J Mater Chem C* 6(45):12121–12141
- Zhang D, Yin R, Zheng Y, Li Q, Liu H, Liu C, Sheng C (2022) Multifunctional MXene/CNTs based flexible electronic textile with excellent strain sensing, electromagnetic interference shielding and Joule heating performances. *Chem Eng J* 438:135587
- Gan L, Shang SM, Yuen CWM, Jiang SX (2015) Graphene nanoribbon coated flexible and conductive cotton fabric. *Compos Sci Technol* 117:208–214
- Xu X, Wu S, Cui J, Yang L, Wu K, Chen X, Sun D (2021) Highly stretchable and sensitive strain sensor based on polypyrrole coated bacterial cellulose fibrous network for human motion detection. *Compos B Eng* 211:108665
- Ummartyotin S, Manuspiya H (2015) A critical review on cellulose: from fundamental to an approach on sensor technology. *Renew Sust Energy Rev* 41:402–412

23. Bu Y, Shen T, Yang W, Yang S, Zhao Y, Liu H, Zheng Y, Liu C, Shen C (2021) Ultrasensitive strain sensor based on superhydrophobic microcracked conductive Ti₃C₂T_x MXene/paper for human-motion monitoring and E-skin. *Sci Bull* 68(18):1849–1857
24. Li Q, Liu H, Zhang S, Zhang D, Liu X, He Y, Mi L, Zhang J, Liu C, Shen C, Guo Z (2019) Superhydrophobic electrically conductive paper for ultrasensitive strain sensor with excellent anticorrosion and self-cleaning property. *ACS Appl Mater Interfaces* 11:21904–21914
25. Correia DM, Ribeiro S, da Costa A, Ribeiro C, Casal M, Lanceros-Mendez S, Machado R (2019) Development of bio-hybrid piezoresistive nanocomposites using silk-elastin protein copolymers. *Compos Sci Technol* 172:134–142
26. Sun L, Liang L, Shi Z, Wang H, Fan R (2020) Optimizing strategy for the dielectric performance of topological-structured polymer nanocomposites by rationally tailoring the spatial distribution of nanofillers. *Eng Sci* 12:95–105
27. Chen X, Liu H, Zheng Y, Zhai Y, Liu X, Liu C, Liu L, Guo Z, Shen C (2019) Highly compressible and robust polyimide/carbon nanotube composite aerogel for high-performance wearable pressure sensor. *ACS Appl Mater Interfaces* 11:42594–42606
28. Zheng Y, Li Y, Zhou Y, Dai K, Zheng G, Zhang B, Liu C, Shen C (2020) High-performance wearable strain sensor based on graphene/cotton fabric with high durability and low detection limit. *ACS Appl Mater Interfaces* 12(1):1474–1485
29. Zhu M, Yu H-y, Tang F, Li Y, Liu Y, Yao J-m (2020) Robust natural biomaterial based flexible artificial skin sensor with high transparency and multiple signals capture. *Chem Eng J* 394:124855
30. He F, You X, Gong H, Yang Y, Bai T, Wang W, Guo W, Liu X, Ye M (2020) Stretchable, biocompatible, and multifunctional silk fibroin-based hydrogels toward wearable strain/pressure sensors and triboelectric nanogenerators. *ACS Appl Mater Interfaces* 12(5):6442–6450
31. Wang Q, Yan S, Han G, Li X, You R, Zhang Q, Li M, Kaplan D (2020) Facile production of natural silk nanofibers for electronic device applications. *Compos Sci Technol* 187:107950
32. Wang D, Zhou X, Song R, Fang C, Wang Z, Wang C, Huang Y, (2021) Freestanding silver/polypyrrole composite film for multifunctional sensor with biomimetic micropattern for physiological signals monitoring. *Chem Eng J* 404:126940
33. Li D, Fan Y, Han G, Guo Z (2020) Superomniphobic Silk Fibroin/Ag nanowires membrane for flexible and transparent electronic sensor. *ACS Appl Mater Interfaces* 12(8):10039–10049
34. Zhou J, Zhao Z, Hu R, Yang J, Xiao H, Liu Y, Lu M (2020) Multi-walled carbon nanotubes functionalized silk fabrics for mechanical sensors and heating materials. *Mater Des* 191:108636
35. Ouyang Z, Xu D, Yu H, Li S, Song Y, Tam K (2022) Novel ultrasonic-coating technology to design robust, highly sensitive and wearable textile sensors with conductive nanocelluloses. *Chem Eng J* 428:131289
36. Dai Z, Wang G, Liu L, Hou Y, Wei Y, Zhang Z (2016) Mechanical behavior and properties of hydrogen bonded graphene/polymer nano-interfaces. *Compos Sci Technol* 136:1–9
37. Kim Y, Choi H, Baek I, Na S (2020) Spider silk with weaker bonding resulting in higher strength and toughness through progressive unfolding and load transfer. *J Mech Behav Biomed* 108:103773
38. Costa CM, Reizabal A, Serra RSI, Balado AA, Perez-Alvarez L, Ribelles JLG, Vilas-Vilela JL, Lanceros-Mendez S (2021) Broadband dielectric response of silk Fibroin/BaTiO₃ composites: influence of nanoparticle size and concentration. *Compos Sci Technol* 213:108927
39. Wantanasiri P, Ratanavaraporn J, Yamdech R, Aramwit P (2014) Fabrication of silk sericin/alginate microparticles by electrohydrodynamic spraying technique for the controlled release of silk sericin. *J Electrostat* 72(1):22–27
40. Meng L, Fu Q, Hao S, Xu F, Yang J (2022) Self-adhesive, biodegradable silk-based dry electrodes for epidermal electrophysiological monitoring. *Chem Eng J* 427:131999
41. Zhu B, Wang H, Leow W, Cai Y, Loh X, Han M, Chen X (2016) Silk fibroin for flexible electronic devices. *Adv Mater* 28(22):4250–4265
42. Liu Y, Tao L, Wang D, Zhang T, Yang Y, Ren T (2017) Flexible, highly sensitive pressure sensor with a wide range based on graphene-silk network structure. *Appl Phys Lett* 110(12):123508
43. Wang S, Ning H, Hu N, Liu Y, Liu F, Zou R, Huang K, Wu X, Weng S, Alamusi, (2020) Environmentally-friendly and multifunctional graphene-silk fabric strain sensor for human-motion detection. *Adv Mater Interfaces* 7(1):1901507
44. Yin R, Yang S, Li Q, Zhang S, Liu H, Han J, Liu C, Shen C (2020) Flexible conductive Ag nanowire/cellulose nanofibril hybrid nanopaper for strain and temperature sensing applications. *Sci Bull* 65(11):899–908
45. Zhang W, Zhang X, Wu Z, Abdurahman K, Cao Y, Duan H, Jia D (2020) Mechanical, electromagnetic shielding and gas sensing properties of flexible cotton fiber/polyaniline composites. *Compos Sci Technol* 188:107966
46. Zhang D, Sun J, Lee LJ, Castro JM (2020) Overview of ultrasonic assisted manufacturing multifunctional carbon nanotube nanopaper based polymer nanocomposites. *Eng Sci* 10:35–50
47. Ma ZL, Wei AJ, Li YT, Shao L, Zhang HM, Xiang XL, Wang JP, Ren QB, Kang SL, Dong DD, Ma JZ, Zhang GC (2021) Lightweight, flexible and highly sensitive segregated microcellular nanocomposite piezoresistive sensors for human motion detection. *Compos Sci Technol* 203:108571
48. Jang G, Hong S, Park H, Lee YH, Park H, Lee H, Jeong YR, Jin S, Keum K, Ha JS (2021) Highly sensitive pressure and temperature sensors fabricated with poly (3-hexylthiophene-2,5-diyl)-coated elastic carbon foam for bio-signal monitoring. *Chem Eng J* 423:130197
49. Lin K, Li Y, Sun J, Zhou D, Zhang Q (2020) Multi-sensor fusion for body sensor network in medical human-robot interaction scenario. *Inf Fusion* 57:15–26
50. Zhang Y, Xie S, Zhang D, Ren B, Zheng J (2019) Thermo-responsive and shape-adaptive hydrogel actuators from fundamentals to applications. *Eng Sci* 6:1–11
51. Enaganti P, Dwivedi P, Srivastava A, Goel S (2020) Analysis of submerged amorphous, mono-and poly-crystalline silicon solar cells using halogen lamp and comparison with xenon solar simulator. *Sol Energy* 211:744–752
52. Ji X, Wang H, Chen T, Zhang T, Chu J, Du A (2020) Intrinsic negative TCR of superblack carbon aerogel films and their ultra-broad band response from UV to microwave. *Carbon* 161:590–598
53. Ji X, Zhong Y, Li C, Chun J, Wang H, Xing Z, Niu T, Zhang Z, Du A (2021) Nanoporous carbon aerogels for laser-printed wearable sensors. *ACS Appl Nano Mater* 4(7):6796–6804

Publisher's Note Springer Nature remains neutral with regard to jurisdictional claims in published maps and institutional affiliations.